Cell Metabolism, Volume *27*

Supplemental Information

The TORC1-Regulated CPA Complex Rewires an RNA Processing Network to Drive Autophagy and Metabolic Reprogramming

Hong-Wen Tang, Yanhui Hu, Chiao-Lin Chen, Baolong Xia, Jonathan Zirin, Min Yuan, John M. Asara, Leonard Rabinow, and Norbert Perrimon

Figure S1. Function of the CPA complex and CPA-interacting splicing factors in autophagy. Related to Figure 2.

(A-B) Identification of polyadenylation sites in 3'UTR of *Atg1* and *Atg8a* by 3'RACE. Position of the polyA sites are indicated by an arrow in the 3'UTR sequences of *Atg1* (A) and *Atg8a* (B). (C) Expression of $Pcf11^{RNAi}$ or Cbc^{RNAi} in the larval fat body induced 3'UTR extension of *Atg1* and *Atg8a* under fed conditions. The ratio between amplicons (Distal 3'UTR/CDS) represents APA isoform changes. (D) Relative mRNA expression of *Atg1* and *Atg8a* transcripts. Compared with control under fed condition (starvation 0 hr), *Atg1* and *Atg8a* mRNAs increased in fat bodies from starved control larva (starvation 4 and 16 hrs), but not from $CPSF6^{RNAi}$, Clp^{RNAi}, or $CstF64^{RNAi}$-expressing larva under starvation for 16 hrs. (E) Long 3'UTRs of *Atg1* and *Atg8a* enhanced protein expression. *Firefly Luciferase* reporters with the indicated 3'UTRs were transfected into S2R+ cells. After 48 hrs, cells were treated with Rapamycin (20 nM) for 24 hrs, followed by measuring Luciferase activity (Student's T-test was performed; data represent as mean ± SEM; *P<0.05, **P<0.01). (F-G) The CPA complex regulates ATG1 and ATG8a protein levels in the larval fat body. Protein extracts from fat bodies of fed or starved larvae with or without Chloroquine (CQ) treatment were subjected to western blot analysis using antibodies as indicated (F). (G) For quantification, the protein levels of ATG1 and ATG8a (with Chloroquine treatment) in each genotype were measured with ImageJ and normalized to the Tubulin levels. Data are expressed as a fold change compared with the wild-type controls under fed condition. One-Way ANOVA test was performed followed by Bonferroni's post hoc test. Measurements shown are mean ± SEM of triplicates; *P<0.05, **P<0.01, ***P<0.001. (H-I) The CPA complex mediates starvation-induced AS of *Atg1* through 9G8 and U2AF50. RNA extracted from larval fat bodies were subjected to RT-PCR analysis to detect the two AS isoforms, *RA* and *RB,* and the long-UTR specific transcripts (Distal 3'UTR) of *Atg1*. Depletion of *Pcf11*, *Cbc,* or *9G8*, induced alternative splicing of *Atg1* isoforms and extended *Atg1* 3'UTR length under fed conditions (H). *Atg1* isoform conversion and

3'UTR length change induced by *Cbc*^{RNAi} was suppressed by co-expressing either *9G8* or *U2AF50*^{RNAi} (I). (J-P) 9G8 and U2AF50 regulate autophagy. Expression of *9G8*^{RNAi} (J) induces mCherry-ATG8a puncta formation in the fed condition. Conversely, expression of *GFP-9G8* (K) or *U2AF50*^{RNAi} (O), but not *SRm300*^{RNAi} (L), *Tra2*^{RNAi} (M), or *Rbp1-like*^{RNAi} (N), repress mChrry-ATG8a puncta formation induced by starvation. (P) Quantification of the relative number of mCherry-ATG8a dots per cell (Student's T-test was performed to identify significant differences between mCherry dot numbers in clones and dot numbers in control cells outside of the clones; data represent the mean± SEM of 3 fat-body samples imaged per genotype; **P<0.01, ***P<0.001). Scale bar, 20 μm. (Q-S) Atg1^{S297A} mutation induced higher autophagic level than wild-type Atg1. More mCherry-ATG8a puncta were induced in clonal expression of *Atg1*^{S297A}, compared to wild-type *Atg1* (M). (N) Quantification of the relative number of mCherry-ATG8a dots per cell (One-Way ANOVA test was performed followed by Bonferroni's post hoc test; data are represented as mean ± SEM; *P<0.05). Protein extracts from the *Atg1-RB*- or *Atg1-RB*^{S297A}-expressing fat bodies of fed larvae with Chloroquine (CQ) treatment were subjected to western blot analysis using antibodies as indicated (S).

Figure S2. The PI3K/AKT/TORC1 pathway regulates APA and AS of *Atg1* and *Atg8a* as well as CPSF6 phosphorylation. Related to Figure 3.

(A-B) Inhibition of the TORC1 signaling induced AS and APA of *Atg1* and *Atg8a*. Larval fat bodies under fed or starved conditions were dissected and subjected to qPCR or RT-PCR analysis using pairs of primers (Figure 2A). *InR*^{RNAi}*, PI3K92E, Pten, PDK1*^{RNAi}*, AKT*^{RNAi}*, Rheb*^{RNAi}*, or TOR*^{RNAi}, induced 3'UTR extension of *Atg1* and *Atg8a* (A) as well as *Atg1* isoforms conversion (B). One-Way ANOVA test was performed followed by Bonferroni's post hoc test. Data are represented as mean ± SEM; *P<0.05, **P<0.01. (C-D) TORC1 activation suppresses CPSF6 phosphorylation. Wild-type, TSC1-KO, or TSC2-KO S2R+ cells transfected with *GFP, GFP-CPSF6, GFP-CPSF160, or GFP-CstF64,* were treated with or without Rapamycin (20 nM) for 24 hrs and then subjected to immunoprecipitation with anti-GFP nanobody. Immunoprecipitated proteins were analyzed by

immunoblotting. The phosphorylation signal of CstF64 was detected, but Rapamycin treatment did not affect it (C). Moreover, the phosphorylation of CPSF6 is repressed in *TSC1-KO* or *TSC2-KO* cells (D).

Figure S3. The CDK8/DOA complex is degraded by TORC1-dependent ubiquitination and interacts with RS domain of CPSF6. Related to Figure 4.

(A) *CDK8/CycC* genetically interacts with *DOA*. Clonal expression of *CDK8* or *DOA* induced mCherry-ATG8a puncta formation in the larval fat body under fed conditions. Depletion of *DOA* or *CycC* can inhibit the CDK8- or DOA-induced effects respectively. Fat body cells are stained with DAPI. (B) Quantification of the relative number of mCherry-ATG8a dots per cell. (One-Way ANOVA test was performed followed by Bonferroni's post hoc test; data are represented as mean ± SEM; ***P<0.001) (C) CDK8 physically interacts with DOA. S2R+ cells, transfected with *Flag-tagged CDK8* and *HA-tagged DOA*. After 48 hrs, cells were treated with Rapamycin (20 nM) for 24 hrs and lysates immunoprecipitated with anti-HA agarose. Immunoprecipitated proteins and total cell lysates (TCL) were analyzed by immunoblotting (IB) with antibodies as indicated. (D) Effects of Rapamycin treatment on the protein levels of CDK8 and DOA. S2R+ cells transfected with *Flag-tagged CDK8* or *HA-tagged DOA* were treated with or without Rapamycin (20 nM) for 24 hrs. Total cell lysates were analyzed by immunoblotting (IB) with antibodies as indicated. (E) TORC1 activity is required for ubiquitination of CDK8 and DOA. S2R+ cells transfected with *Flag-tagged CDK8* or *HA-tagged DOA* were treated with or without Rapamycin (20 nM) in the presence or absence of MG132 (20 μM) for 24hrs and then subjected to immunoprecipitation (IP) with anti-Flag or anti-HA antibodies. Immunoprecipitated proteins and total cell lysates (TCL) were analyzed by immunoblotting (IB). (F) Schematic representation of the domain structures of CPSF6 and RS domain deletion mutants ($CPSF6^{\Delta RS}$). (G-H) CDK8 and DOA physically interact with the RS domain of CPSF6. S2R+ cells, transfected with *GFP, GFP-tagged CPSF6,* or *GFP-tagged*

RS deletion mutant of CPSF6 (CPSF6$^{\Delta RS}$), together with *Flag-tagged CDK8* (L) or *HA-tagged DOA* (M). After 48 hrs, cells were treated with or without Rapamycin (20 nM) for 24 hrs and lysates immunoprecipitated with anti-GFP nanobody. Immunoprecipitated proteins and total cell lysates (TCL) were analyzed by immunoblotting (IB) with antibodies as indicated.

Figure S4. Physiological functions of CPSF6 phosphorylation. Related to Figure 5.

(A) Shown is the amino acid sequence of CPSF6 C-terminal region containing RS domain (401aa - 652aa). The CDK8 consensus phosphorylation sites are indicated by blue boxes and the DOA consensus phosphorylation sites are indicated by red boxes. Purified recombinant CPSF6-C phosphorylated by CDK8 or DOA as described in Figure 2N-O was digested with Chymotrypsin and then subjected to mass spectrometry analysis. The inverted triangles indicate Ser-588 and Ser596 of CPSF6, identified as DOA and CDK8 phosphorylation sites respectively. (B) Quantification of CPSF6 phosphorylation on S588 and S596 residues in vivo. S2R+ cells were transfected with *GFP-CPSF6* with or without Rapamycin (20 nM) and then subjected to immunoprecipitations. The immunoprecipitated CPSF6 proteins were subjected to label-free quantitative mass spectrometry. % occupancy was calculated by dividing the total ion current (TIC) for the phosphorylated peptide by the sum of TIC for both the phosphorylated and unphosphorylated cognate peptide. (C) CDK8 and DOA are required for the Rapamycin-induced phosphorylation of the CPSF6 RS domain. S2R+ cells were treated with dsRNA against LacZ, CDK8, or DOA. After 48 hrs, cells were transfected with *GFP, GFP-CPSF6, GFP-CPSF6^{14A}*, or *GFP-CPSF6$^{\Delta RS}$*, with or without Rapamycin (20 nM) and then subjected to immunoprecipitation. Immunoprecipitated proteins were analyzed by immunoblotting (IB) with antibodies as indicated. (D) TORC1 activity regulates CPSF6 localization. Wild-type, TSC1-KO, or TSC2-KO S2R+ cells, transfected with *GFP* or *GFP-CPSF6,* were treated with or without Rapamycin (20 nM) for 24 hrs and then subjected to immunofluorescence. GFP-CPSF6 was localized in the nuclei of control

cells (wild-type), whereas it redistributed to the cytoplasm in TSC1-KO or TSC2-KO cells. The redistribution of CPSF6 was blocked in TSC1-KO or TSC2-KO cells treated with Rapamycin. Scale bar, 10 mm. (E) TORC1 activity negatively regulates the association between CPSF6 and *Atg* transcripts. Cells were treated as in (D) and then subjected to RNA-immunoprecipitation. Immunoprecipitated RNAs and RNAs of total cell lysates were analyzed by qPCR with pairs of primers (Figure 2A) that detect total transcript (CDS) of *Atg1* or *Atg8a*. Plotted fold change values (ratios of RNA IP/input normalized to GFP control) are the mean ± SEM of triplicates. One-Way ANOVA test was performed followed by Bonferroni's post hoc test; *P<0.05, **P<0.01. (F-H) Phosphorylation of CPSF6 regulates APA and AS of *Atg1* and *Atg8a* transcripts as well as ATG1 and ATG8a protein levels in the larval fat body. Compared with control (starvation 16hrs), expression of CPSF6 with mutations of all fourteen phosphorylatable sites to Alanine ($CPSF6^{14A}$) or CPSF6 carrying a deletion of the RS domain ($CPSF6^{\Delta RS}$) in larval fat body decreased the 3'UTR length of *Atg1* and *Atg8a* transcripts (F), inhibited alternative splicing of *Atg1* isoforms (G), and reduced ATG1 and ATG8a protein levels (H). One-Way ANOVA test was performed followed by Bonferroni's post hoc test; data are represented as mean ± SEM; **P<0.01, ***P<0.001). (I) ATG1 and ATG8a protein were decreased in the larval fat body of CPSF5, CDK8, or DOA mutants. Western blot probed using anti-ATG1, anti-ATG8a, and anti-Tubulin antibodies.

Figure S5. Gene set and protein complex enrichment analyses focusing on autophagy and metabolism. Related to Figure 6.

(A-E) Representative genes involved in energy metabolism (A), ribosome (B), glycolysis (C), autophagy (D), and lipid digestion (E). These biological processes were significantly affected in fat bodies of starved larvae, and the changes could be reversed in fat bodies of starved *CPSF5* mutant larvae. The heat map signals represent the log2 ratio that is normalized to the mean of each gene. Yellow signal denotes higher expression and blue signal denotes lower expression

relative to the mean expression level of each gene. (F) Protein complexes enriched by COMPLEAT analysis related to autophagy, glycolysis, fatty acid biosynthesis, translation, mitochondria, and energy metabolism. For each complex pair, the one on the left represents the expression change in the fat body of 16 hrs starved larvae versus fed larvae while the one on the right represents the expression change in the fat body of 16 hrs starved larvae versus starved *CPSF5* mutants. Each node represents the protein member of each complex with red color for up-regulation or blue color for down-regulation. Edges represent protein-protein interactions. Complexes included at COMPLEAT are either from annotation or prediction (Hu et al., 2017) (G) Relative mRNA expression of genes involved in autophagy and metabolism. RNA extracted from larval fat bodies of fed wt, 16hr-starved wt, 16hr-starved $TSC2^{109}/TSC2^{109}$, 16hr-starved $CDK8^{K185}/Df(3L)AC1$, 16hr-starved DOA^{HD}/DOA^{DEM}, and 16hr-starved $CPSF5^{H11}/CPSF5^{H11}$, were subjected to qPCR analysis to detect gene expression. Compared with control under fed conditions, mRNAs involved in glucose catabolism (*l(1)G0334* and *Eno*), ribosome (*mRpL49, mRpL16,* and *mRpL17*) or energy metabolism (*ATPsynδ, ATPsynD, ND-MWFE,* and *ND-13A*) decreased in fat bodies from starved larvae, but not from *Tsc2, CDK8, DOA,* or *CPSF5* mutant larvae starved for 16 hrs. In contrast, mRNAs involved in autophagy (*Atg7* and *br*) and lipid catabolism (*Npc1a* and *Sdc*) increased in fat bodies from 16hr-starved larva, but not from *Tsc2, CDK8, DOA,* or *CPSF5* mutant larva starved for 16 hrs. *SRPK* mRNA did not show significant changes in any condition. One-Way ANOVA test was performed followed by Bonferroni's post hoc test. Measurements shown are mean ± SEM; *P<0.05, **P<0.01, ***P<0.001. (H) CDK8, DOA, and CPSF6 regulate lipid metabolism. Clonal expression of $CPSF6^{RNAi}$, DOA^{RNAi}, or $CDK8^{RNAi}$ in GFP-ATG8a labeled cells increased the size of lipid droplets stained by Nile red upon starvation. Scale bar, 20 μm. Quantification of the relative intensity of Nile red signals is shown (Student's T-test was performed to identify significant differences between Nile red signals in clones and signals in control cells outside of the clones; data represent as the mean± SEM of 3 fat-body samples imaged per genotype; *P<0.05, **P<0.01).

Figure S6. CDK8 and CLK2 interact with and phosphorylate CPSF6 to control its localization, RNA-binding ability, and autophagy in mammalian cells. Related to Figure 7.

(A) Human CPSF6 physically interacts with CDK8 and CLK2 under starvation conditions. HEK293T cells, transfected with GFP or GFP-tagged CPSF6, were incubated in nutrient rich medium (DMEM) or starvation medium (EBSS) for 2 hrs and subjected to immunoprecipitation (IP) with an anti-GFP nanobody. Immunoprecipitates and total cell lysates (TCL) were analyzed by immunoblotting (IB). (B) CDK8 and CLK2 are required for the starvation-induced phosphorylation of human CPSF6. Cells were cultured in DMEM or EBSS in the presence or absence of 50 μM Senexin-A (CDK8 inhibitor) or 50 μM TG003 (CLK2 inhibitor) for 2 hrs and then subjected to immunoprecipitation (IP). Immunoprecipitates and total cell lysates (TCL) were analyzed by immunoblotting (IB). (C) The CDK8 and CLK2-mediated phosphorylation of CPSF6 is essential for its association with RNAs. HEK293T cells transfected with GFP or GFP-CPSF6 were cultured in nutrient rich medium (DMEM) or starvation medium (EBSS) in the presence or absence of 50 μM Senexin-A (CDK8 inhibitor) or 50 μM TG003 (CLK2 inhibitor) for 2 hrs, and then subjected to RNA immunoprecipitations. Immunoprecipitated RNAs and RNAs of total cell lysates were analyzed by qRT-PCR with pairs of primers against *ULK1* and *LC3B.* Plotted fold change values (ratios of RNA IP/input normalized to GFP control) are the mean ± SEM of triplicates. One-Way ANOVA test was performed followed by Bonferroni's post hoc test. *P<0.05, **P<0.01. (D) Phosphorylation of CPSF6 by CDK8 or CLK2 is required for its nuclear targeting. MCF7 cells were cultured in DMEM or EBSS in the presence or absence of 50 μM Senexin-A (CDK8 inhibitor) or 50 μM TG003 (CLK2 inhibitor) for 2 hrs and then subjected to immunofluorescence analysis. CPSF6 was enriched in nuclei under fed or starvation conditions, whereas it redistributed to the cytoplasm when cells were treated with Senexin-A or TG003. Cells are stained with DAPI (blue). Scale bar, 10 mm. (E-F) CDK8, CLK2, and CPSF6 are required for

starvation-induced autophagosome formation. MCF7 cells were cultured in nutrient rich medium (DMEM) or starvation medium (EBSS) in the presence or absence of the lysosomal inhibitor Bafilomycin A1 (BafA1) for 2 hrs and subjected to immunofluorescence analysis. Compared to the nutrient rich conditions, the number of LC3 punctae were increased by starvation. Treatment of 50 μM Senexin-A (CDK8 inhibitor) or 50 μM TG003 (CLK2 inhibitor) (E), or infection with lentivirus expressing *CPSF6* shRNA (F) inhibited EBSS-induced LC3 punctae formation. shLuc is used as control. LC3 was stained with LC3B antibody (green) and nuclei were stained with DAPI (blue). Scale bar, 10 μm.

Figure S7. Model of autophagy and metabolism regulation by TORC1/CDK8/DOA/CPA. Related to Figure 7.

(A-B) TORC1 promotes the ubiquitination and degradation of CDK8 and DOA/CLK2 (A). In response to nutrient deprivation, where TORC1 activity is reduced, CDK8 and DOA/CLK2 protein levels are up-regulated, which in turn leads to CPSF6 phosphorylation that enhances its RNA binding ability and promotes APA and AS of transcripts related to autophagy and metabolism. APA-induced *Atg1-RA* transcripts possess long 3'UTRs that stabilize them. In addition, AS-induced *Atg1-RA* transcripts encode a kinase that escapes the inhibition by PKA, thus leading to induction of autophagy. These alternate RNA processing events also suppress lipid, protein, and energy metabolism (B). (C) Moreover, as TORC1 is hyperactivated, CPSF6 phosphorylation is blocked and CPSF6 translocates to the cytoplasm, further inhibiting autophagy and enhancing lipid, protein, and energy metabolism.

Figure S1

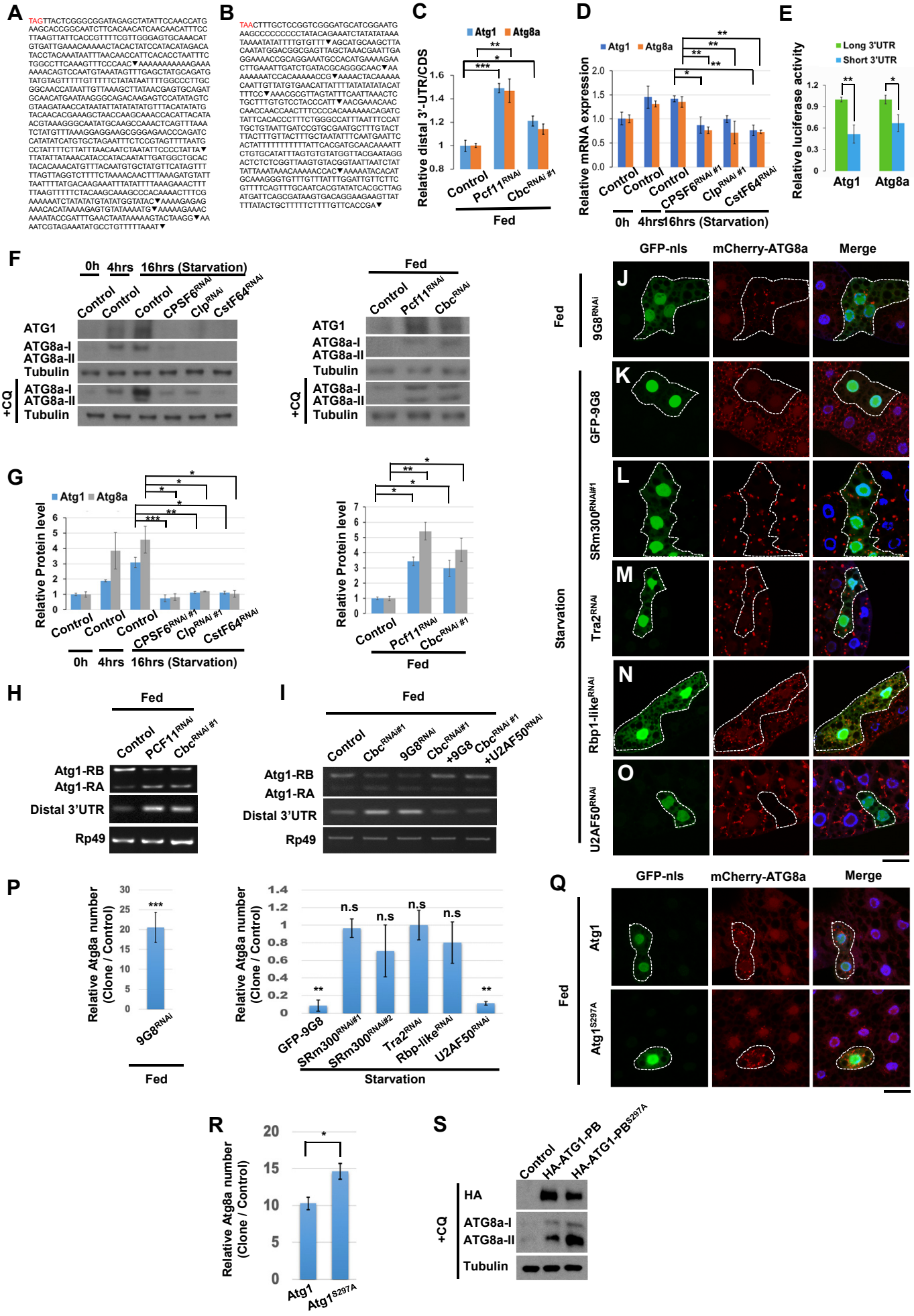
A
B
C
Atg1
Atg8a
Relative distal 3'-UTR/CDS
Control
Pcf11RNAi
CbcRNAi #1
Fed
D
Relative mRNA expression
Control
CPSF6RNAi #1
ClpRNAi #1
CstF64RNAi
0h
4hrs
16hrs (Starvation)
E
Long 3'UTR
Short 3'UTR
Relative luciferase activity
F
ATG1
ATG8a-I
ATG8a-II
Tubulin
+CQ
G
Relative Protein level
H
Atg1-RB
Atg1-RA
Distal 3'UTR
Rp49
PCF11RNAi
I
CbcRNAi#1
9G8RNAi
CbcRNAi#1 +9G8
CbcRNAi #1 +U2AF50RNAi
J
GFP-nls
mCherry-ATG8a
Merge
9G8RNAi
K
GFP-9G8
L
SRm300RNAi#1
M
Tra2RNAi
N
Rbp1-likeRNAi
O
U2AF50RNAi
Starvation
P
Relative Atg8a number (Clone / Control)
n.s
GFP-9G8
SRm300RNAi#1
SRm300RNAi#2
Tra2RNAi
Rbp-likeRNAi
U2AF50RNAi
Q
Atg1
Atg1S297A
R
S
HA-ATG1-PB
HA-ATG1-PBS297A
HA

Figure S2

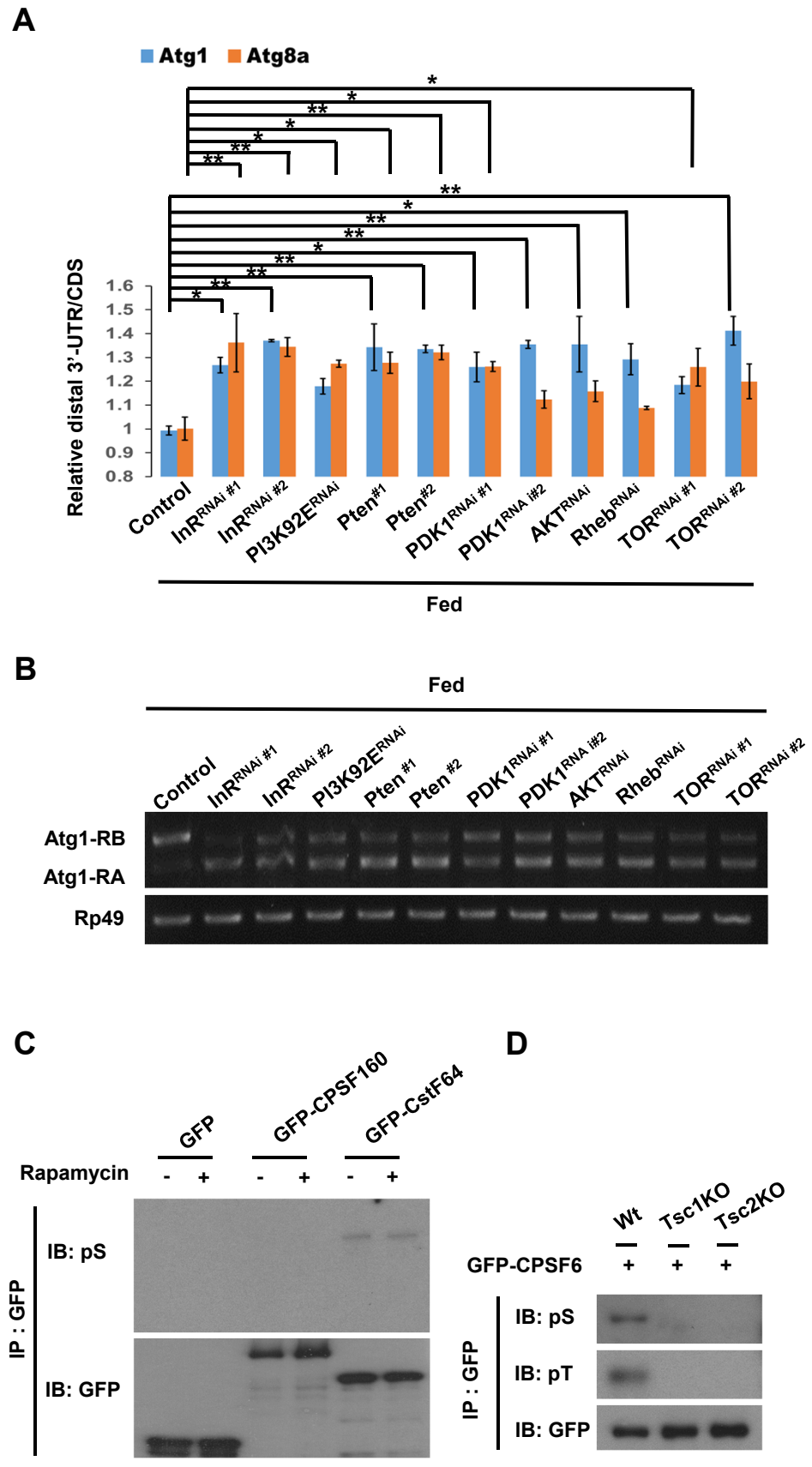
A
Atg1
Atg8a
Relative distal 3'-UTR/CDS
1.6
1.5
1.4
1.3
1.2
1.1
1
0.9
0.8
Control
InR RNAi #1
InR RNAi #2
PI3K92E RNAi
Pten #1
Pten #2
PDK1 RNAi #1
PDK1 RNA i#2
AKT RNAi
Rheb RNAi
TOR RNAi #1
TOR RNAi #2
Fed
B
Fed
Control
InR RNAi #1
InR RNAi #2
PI3K92E RNAi
Pten #1
Pten #2
PDK1 RNAi #1
PDK1 RNA i#2
AKT RNAi
Rheb RNAi
TOR RNAi #1
TOR RNAi #2
Atg1-RB
Atg1-RA
Rp49
C
GFP
GFP-CPSF160
GFP-CstF64
Rapamycin
- + - + - +
IP : GFP
IB: pS
IB: GFP
D
Wt
Tsc1KO
Tsc2KO
GFP-CPSF6
+ + +
IP : GFP
IB: pS
IB: pT
IB: GFP

Figure S3

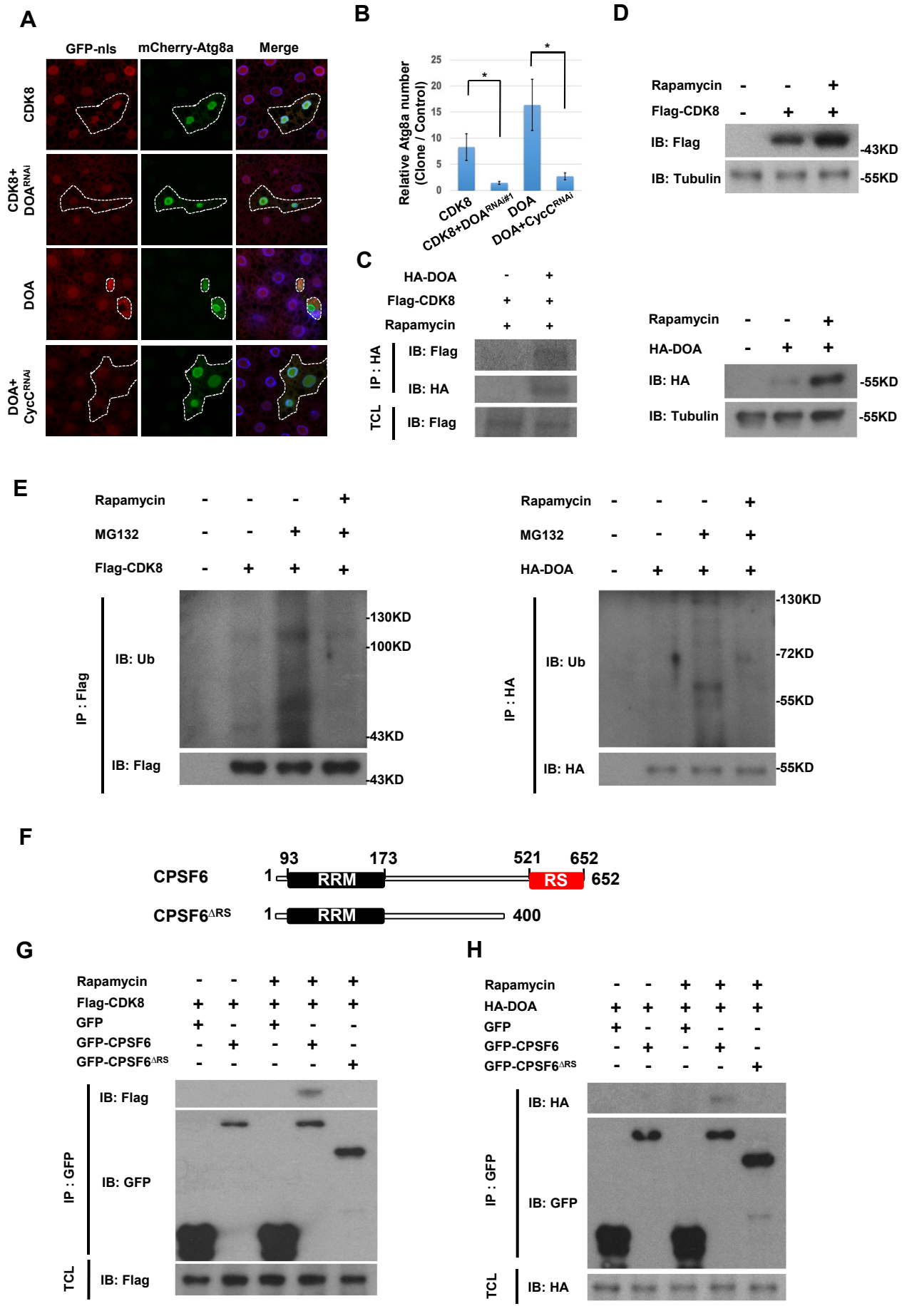
A
GFP-nls
mCherry-Atg8a
Merge
CDK8
CDK8+ DOA^RNAi
DOA
DOA+ CycC^RNAi
B
Relative Atg8a number (Clone / Control)
25
20
15
10
5
0
*
*
CDK8
CDK8+DOA^RNAi#1
DOA
DOA+CycC^RNAi
C
HA-DOA - +
Flag-CDK8 + +
Rapamycin + +
IP : HA
IB: Flag
IB: HA
TCL
IB: Flag
D
Rapamycin - - +
Flag-CDK8 - + +
IB: Flag
-43KD
IB: Tubulin
-55KD
Rapamycin - - +
HA-DOA - + +
IB: HA
-55KD
IB: Tubulin
-55KD
E
Rapamycin - - - +
MG132 - - + +
Flag-CDK8 - + + +
IP : Flag
IB: Ub
-130KD
-100KD
-43KD
IB: Flag
-43KD
Rapamycin - - - +
MG132 - - + +
HA-DOA - + + +
IP : HA
IB: Ub
-130KD
-72KD
-55KD
IB: HA
-55KD
F
CPSF6
1
93
173
521
652
RRM
RS
652
CPSF6^ΔRS
1
RRM
400
G
Rapamycin - - + + +
Flag-CDK8 + + + + +
GFP + - + - -
GFP-CPSF6 - + - + -
GFP-CPSF6^ΔRS - - - - +
IP : GFP
IB: Flag
IB: GFP
TCL
IB: Flag
H
Rapamycin - - + + +
HA-DOA + + + + +
GFP + - + - -
GFP-CPSF6 - + - + -
GFP-CPSF6^ΔRS - - - - +
IP : GFP
IB: HA
IB: GFP
TCL
IB: HA

Figure S4

A

Drosophila CPSF6 (401aa - 652aa)

MNMTPQHGPP PQFAQHGPRG PWPPPQGKPP GPFPDPQQMG PQLTEVEFEE
VMSRNRTVSS SAIARAVSDA AAGEYSSAIE TLVTAISLIK QSKVAHDERC
KILISSLQDT LHGIEAKSYN RRERSRSRER SHRSRQRRER STSRYRERSR
ERERDRDRER ERDGGSYRER SRSRERERQA PDHYRDDSRS VRPRKSPEPV
VAEAAEAPSS KRYYEDRERY RSSDRERRDR DRDRDRERER DRDRREEHRS
RH

S588 S596

: CDK8 consensus phosphorylation sites
: DOA consensus phosphorylation sites
: CDK8 phosphorylation site identified in in-vitro kinase assay
: DOA phosphorylation site identified in in-vitro kinase assay

B

	Peptide sequence	DMSO		Rapamycin	
		Total-ion-current	Occupancy	Total-ion-current	Occupancy
pS588 S588	RDDpSRSVRPRKSPEPVVAEAAEAPSSKRY RDDSRSVRPRKSPEPVVAEAAEAPSSKRY	0 7473527.7	0%	210073 5009806.6	4.02%
pS596 S596	RDDSRSVRPRKpSPEPVVAEAAEAPSSKRY RDDSRSVRPRKSPEPVVAEAAEAPSSKRY	3422309.5 4051218.2	45.79%	3176605 2043274.6	60.86%

C

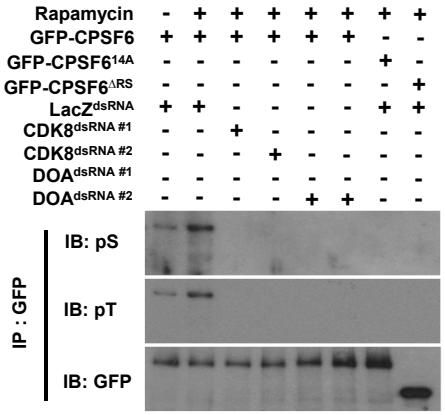

D

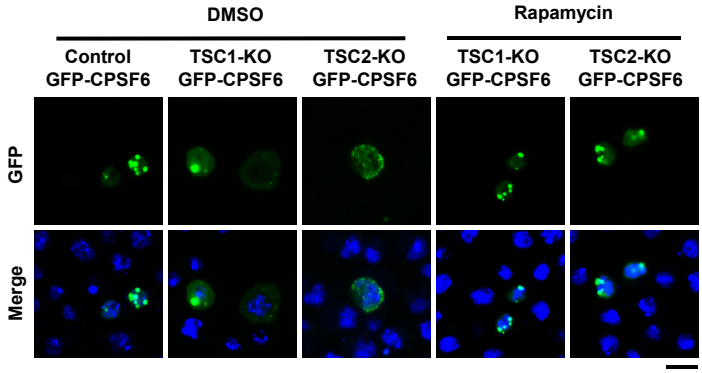

E

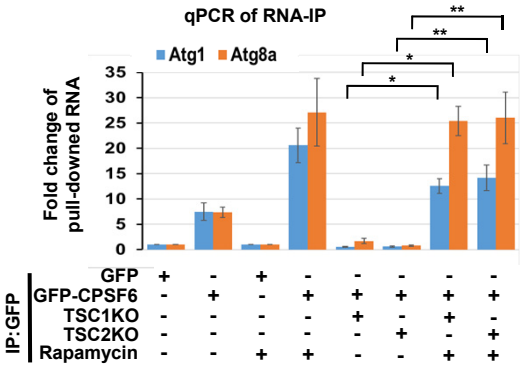

F

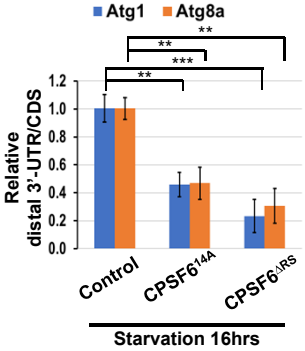

G

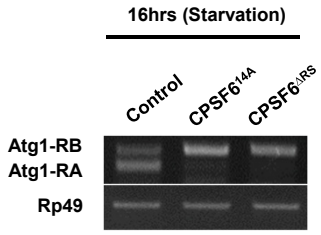

H

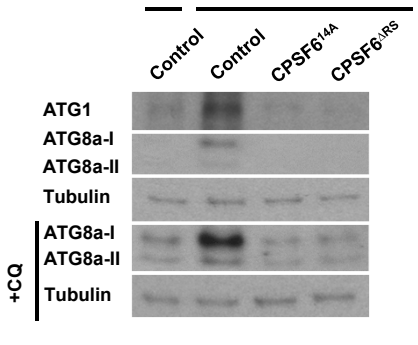

I

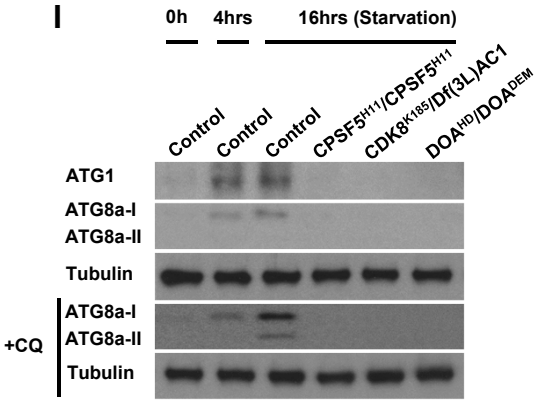

Figure S5

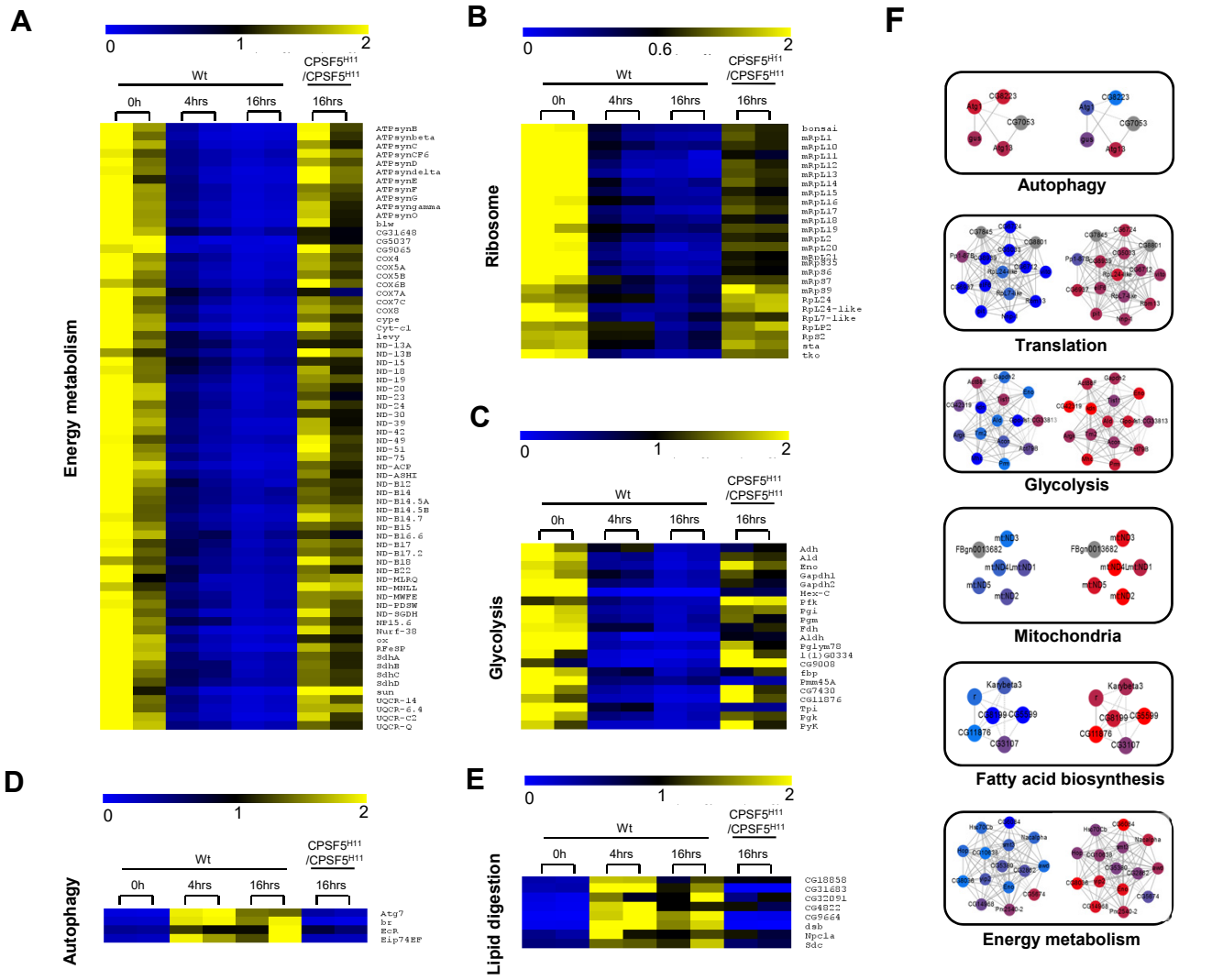
A
B
C
D
E
F
Wt
CPSF5H11 /CPSF5H11
0h
4hrs
16hrs
Energy metabolism
Ribosome
Glycolysis
Autophagy
Lipid digestion
Autophagy
Translation
Glycolysis
Mitochondria
Fatty acid biosynthesis
Energy metabolism

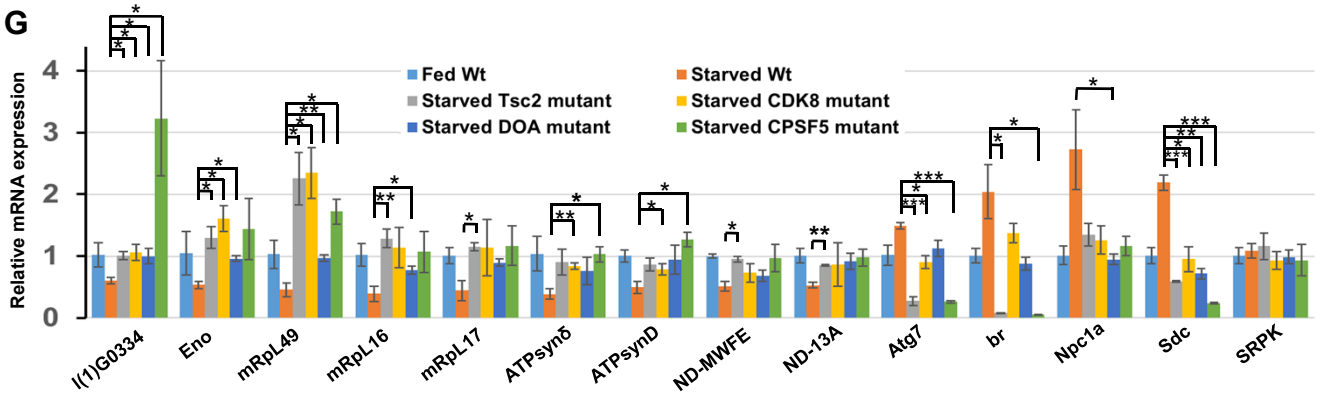
G
Relative mRNA expression
Fed Wt
Starved Wt
Starved Tsc2 mutant
Starved CDK8 mutant
Starved DOA mutant
Starved CPSF5 mutant
l(1)G0334
Eno
mRpL49
mRpL16
mRpL17
ATPsyn5
ATPsynD
ND-MWFE
ND-13A
Atg7
br
Npc1a
Sdc
SRPK

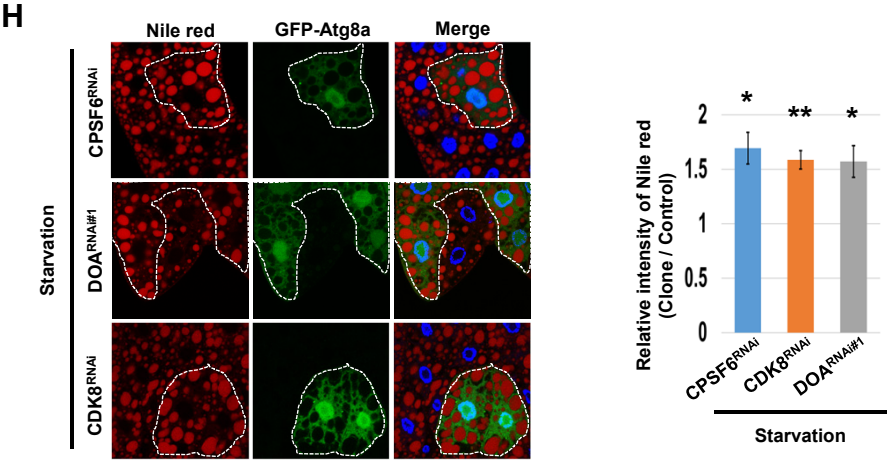
H
Nile red
GFP-Atg8a
Merge
Starvation
CPSF6RNAi
DOARNAi#1
CDK8RNAi
Relative intensity of Nile red (Clone / Control)
Starvation

Figure S6

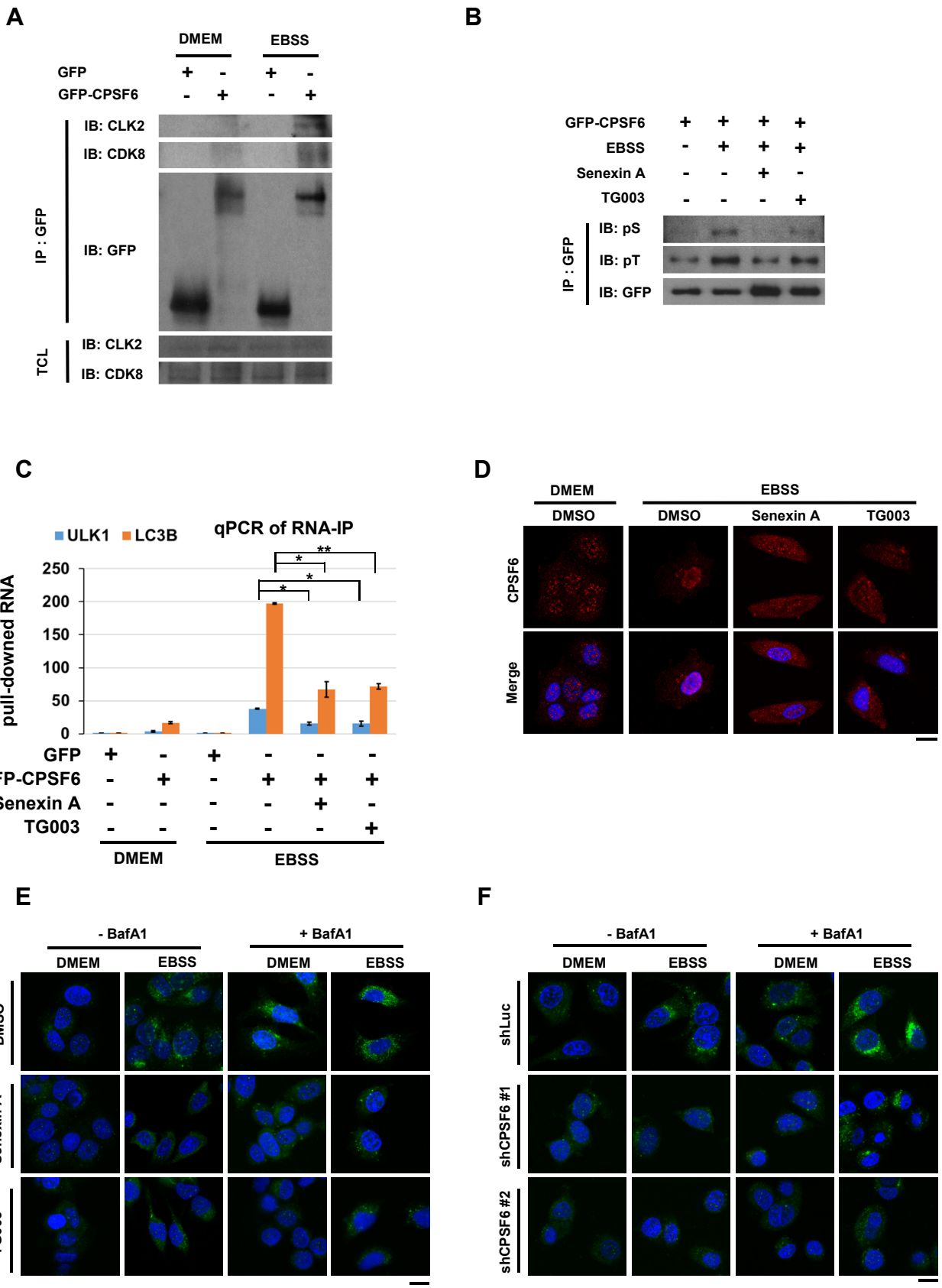
A
DMEM
EBSS
GFP
GFP-CPSF6
IB: CLK2
IB: CDK8
IB: GFP
IP : GFP
TCL
IB: CLK2
IB: CDK8
B
GFP-CPSF6
EBSS
Senexin A
TG003
IB: pS
IB: pT
IB: GFP
IP : GFP
C
ULK1
LC3B
qPCR of RNA-IP
Fold change of pull-downed RNA
250
200
150
100
50
0
GFP
GFP-CPSF6
Senexin A
TG003
IP:GFP
DMEM
EBSS
D
DMEM
EBSS
DMSO
DMSO
Senexin A
TG003
CPSF6
Merge
E
- BafA1
+ BafA1
DMEM
EBSS
DMEM
EBSS
DMSO
Senexin A
TG003
F
- BafA1
+ BafA1
DMEM
EBSS
DMEM
EBSS
shLuc
shCPSF6 #1
shCPSF6 #2

Figure S7

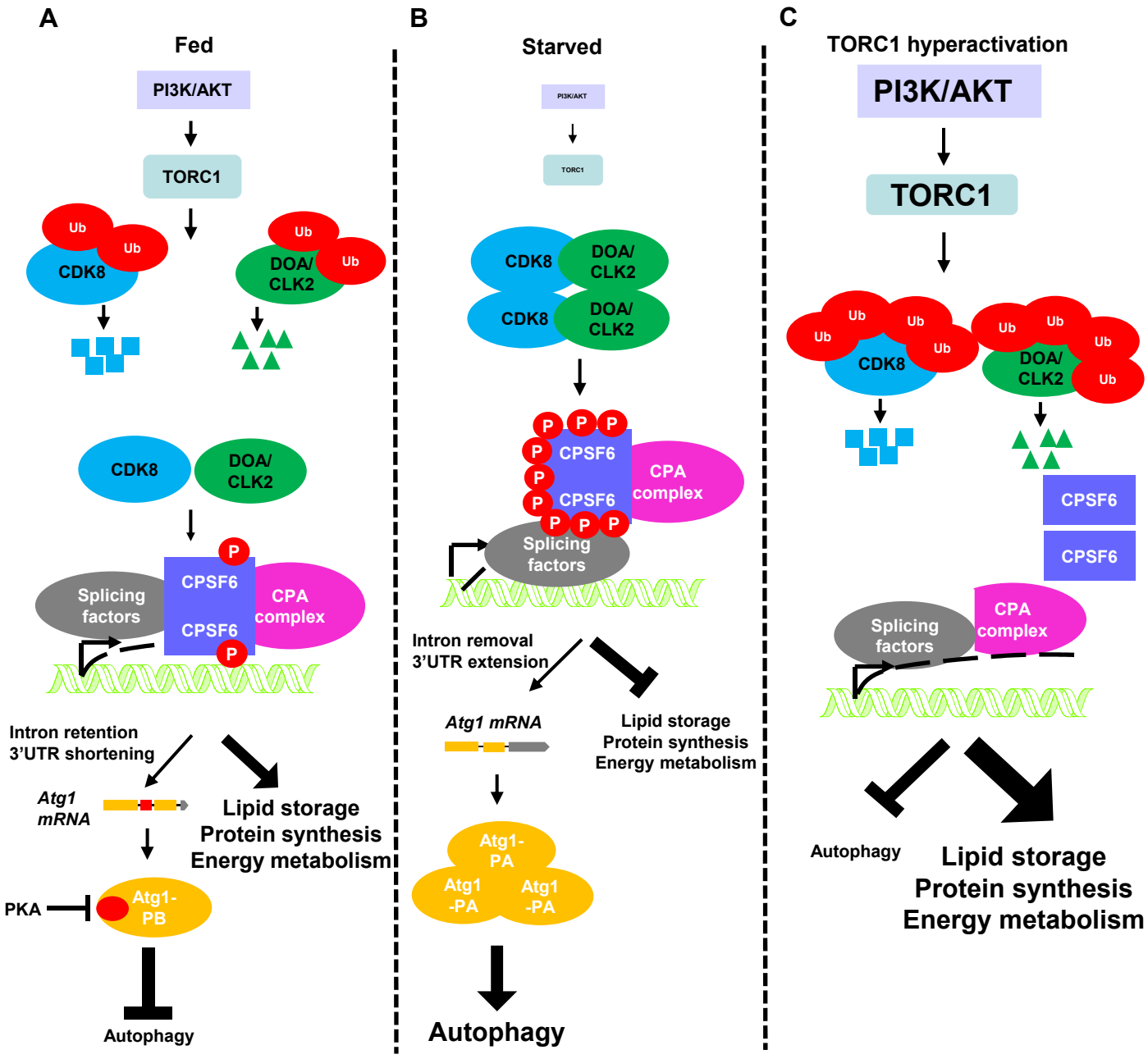
A
Fed
PI3K/AKT
TORC1
Ub
CDK8
DOA/
CLK2
CPSF6
CPA
complex
Splicing
factors
P
Intron retention
3'UTR shortening
Atg1
mRNA
Lipid storage
Protein synthesis
Energy metabolism
PKA
Atg1-
PB
Autophagy
B
Starved
Intron removal
3'UTR extension
Atg1 mRNA
Atg1-
PA
Atg1
-PA
Lipid storage
Protein synthesis
Energy metabolism
Autophagy
C
TORC1 hyperactivation
PI3K/AKT
TORC1
CPSF6
Autophagy
Lipid storage
Protein synthesis
Energy metabolism